SHALLOW CRACK EFFECT ON FRACTURE TOUGHNESS IN A LOW ALLOY STEEL

D.Tigges*, R.Piques*, J.-M. Frund** and A.Pineau*

Fracture mechanics tests carried out at low temperature on a C-Mn-Ni-Mo steel show that the ductile-brittle transition temperature is shifted to lower temperatures for shallow cracks ($\approx$ 1mm), as compared to conventional deeply cracked specimens. This behaviour is quantitatively explained by using the results of the Beremin theory for brittle fracture based on the Weibull statistical approach. It is numerically shown that the shift in the transition temperature is related to the loss of constraint effect due to large scale yielding (LSY) that takes place at relatively low temperatures for shallow cracks.

INTRODUCTION

Classical fracture mechanics theory assumes that a single parameter, such as the stress intensity factor, K, the J contour integral, or the crack tip opening displacement (CTOD), uniquely defines the conditions at the crack tip. A critical value of K, J or CTOD at fracture (i.e. the fracture toughness) is assumed to be a material constant. When this single parameter assumption is valid, laboratory fracture toughness tests can be used to predict the fracture behaviour of large structures. The transferability of fracture mechanics test results, however, is problematic in a number of situations, in particular, because of the shallow crack effect. It is usually observed that the transition temperature is shifted to lower temperatures for shallow cracks, see e.g. (1-4). Therefore the use of lower-bound toughness values from deeply notched specimens may be unacceptable, because overly conservative, to insure a level of quality in a large structure. The main explanation of this geometrical dependence of fracture toughness relies upon the fact that the classical fracture mechanics approach does not account for the loss in crack tip triaxiality that occurs under large scale yielding (LSY) conditions in geometries containing shallow cracks. A number of researchers have recently developed approaches to account for these loss of constraint effects associated

* Centre des Matériaux, Ecole des Mines de Paris, BP 87, 91003 Evry-Cedex, FRANCE, URA CNRS n°866
** Centre de Recherches des Renardières, EDF, BP 1, 77250 Morêt sur Loing

with geometrical effects. Most of these methodologies can be classified as either global or local approaches. The global (or continuum) approaches, see e.g. (5-8), introduce a second parameter (T or Q) to characterize crack tip triaxiality. The local (or micromechanical) approaches, see e.g. (9,10), attempt to predict the effect of crack tip constraint on fracture toughness by performing a stress analysis (analytical or numerical) at the crack tip and applying a local failure criterion.

In the present study the local approach initially developed by the Beremin group (11) is applied to account for the shallow crack effect observed in a low alloy steel. In this theory which is based on the Weibull weakest link concept, see also Wallin et al. (12), the probability of failure, P_r, of a specimen of volume, V, subjected to an homogeneous stress state is given by:

$$P_r=1\text{-}\exp[-\sigma_1^m V/(\sigma_u^m V_u)] \tag{1}$$

where σ_1 is the maximum principal stress, V_u is an abritary elementary volume (in the following, $V_u=(50\mu m)^3$), σ_u is the average cleavage strength of that volume, while m is the Weibull shape factor which describes the scatter in the results. Eq. 1 is a simplified expression since no cut-off parameter is introduced. In three dimensions and in the presence of smooth stress gradients, this equation can be expressed as:

$$P_r=1\text{-}\exp[-\int_{PZ}(\sigma_1^m dV)/(\sigma_u^m V_u)] \tag{2}$$

where the volume integral is extended over the plastic zone PZ. The latter expression can be rewritten as:

$$\sigma_w^m=\int_{PZ}\sigma_1^m dV/V_u=\sigma_u^m \ln[1/(1-P_r)] \tag{3}$$

where σ_w is referred to as the "Weibull stress". For small scale yielding (SSY) conditions it was shown earlier that Eq. 3 can be expressed analytically as:

$$\ln[1/(1-P_r)]=\sigma_w^m/\sigma_u^m=J_{1c}^2E^2B^2\sigma_0^{m-4}C_m/((1-\nu^2)^2V_u\sigma_u^m) \tag{4}$$

where B is the specimen thickness, E the Young modulus, σ_0 the yield strength, C_m is a numerical factor, function of the work hardening exponent ($\sigma=k\epsilon^n$) and of the shape factor, m, while

$$J_{1c}^2=K_{1c}^2(1-\nu^2)/E \tag{5}$$

The influence of the loss of constraint effect due to LSY conditions for deep cracks was investigated numerically in Ref. (13), see Fig. 1. In this figure it is observed that the decrease in stress triaxiality associated to LSY conditions produces a curvature on the $\ln\ln[1/(1-Pr)]$-$\ln(J/\sigma_0)$ plot. The deviation from the

SSY solution is function of crack length and temperature, as indicated schematically in Fig. 1. In the present study devoted to shallow cracks loaded by bending the crack tip triaxiality may be lost by yielding to the top surface containing the crack. This will produce an increase in the fracture toughness, as shown schematically in Fig. 1.

EXPERIMENTAL PROCEDURES

The shallow crack effect can easily be shown by comparing the toughness data from deep cracks to those from shallow crack specimens tested in the transition temperature regime. Typical deeply cracked specimens are the CT specimens. Former work was based on conventional CT specimens with a width of 25, 50 and 195mm taken from a rolled product of 200mm thickness. The steel of the analysed plate corresponds to the American standard A508 Cl 3. It is a quenched and tempered low alloy steel which is largely used for nuclear constructions with a bainitic microstructure having a grain size of about 30μm. The variation of fracture toughness as a function of temperature was determined, (14). The shallow crack specimens were taken from the same product and tested in the same orientation. In Table 1 and 2 we give a brief chemical and mechanical characterisation of the steel.

The crack length effect was investigated with 4 point bend specimens with a span of about 52.5mm. Between the loading frame and the specimen, 4 small cylinders were placed to avoid introducing an additional load tangential to the

TABLE 2 Chemical composition (Wt. Pct.)

Element	C	Mo	Mn	Ni	Cr
weight %	0.195	0.53	1.61	0.82	0.19
Element	Si	Cu	Al	S	P
weight %	0.28	0.065	0.03	0.003	0.012

TABLE 1 Mechanical Properties

ϑ, (°C)	σ_0, (MPa)	UTS, (MPa)	A, (%)	k, MPa ($\sigma=k\epsilon_{pl}^{n}$)	n
20	618	745	19	-	-
-90	711	903	13	1131.6	0.1
-130	776	933	11	1232.9	0.1

specimen. The specimens were precracked up to a crack thickness ratio a/W=0.5. The samples which were finally tested were taken from the precracked specimens in such a way that the mid-section becomes 20mm x 20mm with a ratio a/W≅0.1, (Fig. 2). The specimens were tested in the T L direction. The fracture tests were carried out under displacement control at different temperatures, between -196°C and -100°C. At fracture, the applied load, the load-line displacement and the displacement of a clip-gage were registered. The clip gage measured the displacement of two knifes situated each at a distance of 2mm from the crack mouth.

NUMERICAL CALCULATIONS

The main details of the FE-calculations are given in Table 3. 8 nodes quadrilateral elements with reduced integration for plane deformation were used with large deformation theory. The blunted crack tip is modelled by a finite crack tip radius as proposed by Mc Meeking, (15).

Fig. 3 shows the details of the FE-mesh used to model the behaviour of one shallow crack specimen. This figure shows the contour which was used to calculate J_{1c}.

Fig. 4 compares the distribution of the stresses ahead of the crack tip calculated numerically (T84-10 specimen) with those determined from the Hutchinson-Rice-Rosengreen HRR-field, (16). A significant difference between both fields is noticed. This difference can be measured by the Q factor introduced by Shih, (8). At a distance of $3J/\sigma_0$ from the crack tip the average value of Q inferred from Fig. 4 is found to be of the order of 0.79 which compares well with the Shih estimates for 3 point bend specimens of 0.78.

TABLE 3 Main details of FE-calculations

Code	ABAQUS, plane deformation, large deformation theory
Structure	Element type CPE8R, 323 elements, 1074 nodes, , Size of smallest element at the crack tip≈crack tip radius= 1, 6.5, 13, and 80μm (specimen dependent)
Loading	Displacement control, loading applied to one node in a coarse surrounding mesh

RESUTS

16 shallow crack specimens with a/W values between 0.02 and 0.15 were tested (Table 4). In this table the test conditions (thickness B; a/W ratio; test temperature, ϑ; load at fracture, P_f) and the values of K_{1Jc} determined from Eq. 5 are given. Fractographic examinations showed that, in most cases, fracture occurred by cleavage, except in two specimens (T84-16 and T84-17) which contained a significant amount of intergranular facets in addition to the cleavage facets. The results of all these tests are reported on Figure 5 (■). These tests results show a large scatter in the data and that the fracture toughness increases dramatically above -150°C.

The results obtained on 19 CT type specimens tested in Ref. (14) are reported in Fig. 5, too. These tests were carried out over the temperature range between -125°C and R.T.. Only 6 specimens fulfilled the conditions for valid K_{1C} measurements. For the other ones, the fracture toughness was determined from Eq. 5 using the procedures of the ASTM standards (17) for the determination of

TABLE 4 Experimental Results

Spec.	ϑ, (°C)	B, (mm)	P_f, (kN)	a/W -	K_{1Jc} (MPa$\sqrt{m}$)	σ_w, m=22 (MPa)	P_r, σ_u= 2600MPa
T84-1	-180	23.5	21.25	0.15	37.4	2935.9	0.999
T84-3	-100	22	74.5	0.104	109.7	2448.7	0.235
T84-5	-196	23	18.75	0.13	34.0	2809.0	0.996
T84-6	-100	21.9	35.5	0.081	74.6	2300.0	0.065
T84-7	-90	20.6	72.0	0.062	262.2	2400.0	0.158
T84-8	-130	21.1	67	0.053	109.5	2754.2	0.206
T84-9	-120	17.8	26.25	0.052	64.4	2438.5	0.052
T84-10	-140	20	47.38	0.07	92.4	2523.1	0.403
T84-11	-110	20.9	77.32	0.05	155.0	2817.8	0.243
T84-12	-120	21	61.0	0.078	104.0	2439.0	0.217
T84-13	-130	20.9	53.75	0.083	81.9	2428.0	0.199
T84-14	-140	18.8	47.38	0.04	106.1	2401.0	0.159
T84-15	-100	20.9	65.0	0.062	160.6	2454.0	0.244
T84-16	-150	19.3	50.38	0.017	138.4	2241.0	0.037
T84-17	-160	20.4	26.83	0.04	85.5	2441.0	0.221
T84-18	-150	22	83.43	0.02	111.7	2497.1	0.337

J_{1c}. These test results show also a large scatter in the data. Furthermore the fracture toughness increases smoothly with temperature, especially above -80°C. A significant shift in transition temperature is observed when the long crack results are compared to those obtained on shallow cracks. At K = 100MPa$\sqrt{m}$ this shift is of the order of 60°C. These results therefore illustrate in this material the shallow crack effect on fracture toughness.

DISCUSSION

The experimental results obtained in this study clearly confirm that the global approach of fracture mechanics based on a single loading parameter is unable to describe the shallow crack effect. In this discussion an attempt is made to show that the local approach predicts this effect in a better way.

For SSY conditions which are prevailing in the tests performed on CT specimens and on shallow cracks at very low temperatures the analytical expression given in Eq. 4 can be applied. From this theoretical expression a value for m=22 was inferred. This value had already been found on a similar steel, but using then a widely different procedure based on tests with notched specimens, (11). With this value of m, keeping $V_0=(50\mu m)^3$ and $\sigma_u=2600MPa$ which is also a value found elsewhere (11) it is possible to calculate the probability to failure for $P_r=0.1$ and $P_r=0.9$, provided that the value of C_m is known. This is shown in Fig. 5 where it is observed that these calculated values for P_r account for the scatter observed on deeply cracked specimens. The calculations were made using the values of C_m given in Reference (11) divided by a factor of 60. But it is clear that in Eq. 4, the values of C_m and σ_u^m are related. Independent measurements of σ_u are necessary before further discussion of the value used for C_m parameter. At the present stage of this study it should be emphasized that Eq. 4 predicts correctly the variation of the fracture toughness of deeply cracked specimens, tested under predominant SSY conditions, with temperature.

These values of the local approach parameters (m, σ_u and V_u) were then used to calculate the Weibull stress (Eq. 3) for the shallow cracks and therefore the probability to failure. Fig. 4 shows that the maximum principal stress, σ_1, is reduced at fracture for shallow cracks. The loss of constraint is reflected by a reduced principal stress and, on the other side, by an increased plastic zone size. The shallow crack effect results from a counter-balancing effect between the reduction in σ_1 and the increase of the plastic zone size, as indicated by Eq. 2. However, the large value of the m exponent in this equation is such that the stress effect is the most important. The results are reported in Table 4 where one notices that, in all cases, the values predicted for the probability to failure are reasonable. In particular it is noticed that the specimen T84-16 in which some intergranular fracture was observed gives rise to a low probability to failure. This is consistent with the fact that the fracture toughness associated with this mode of failure is

lower than the toughness corresponding to cleavage. The same effect is observed in T84-17, although less pronounced, since $P_r=0.22$. The FEM calculations were performed for each specimen. In Fig. 5 we have reported the probabilities to failure of $P_r=0.1$ and $P_r=0.9$ inferred from this type of calculation corresponding to $a/W=0.07$ which is representative of the used average values for the a/W ratio. It is observed that most of the experimental results obtained on shallow cracks are included within this calculated scatter band. A close examination shows that the results of specimens T84-3 and T84-6 are located on the right handside of the scatter line corresponding to $P_r=0.1$. Table 4 shows that for these specimens $a/W>0.07$, such as the shallow crack effect tends to be reduced. It is also worth noting that the results obtained on specimen T84-18 are above the $P_r=0.9$ scatter line. Table 4 shows that, in this case, $a/W=0.02$ which is much lower than 0.07. The shallow crack effect is therefore reinforced. The situation observed for T84-16 and T84-17 specimen is specific in the sense that there is a counter-balancing effect between intergranular brittleness and the shallow crack effect.

CONCLUSION

1.) In a A508 Cl 3 steel the ductile-brittle transition temperature is shifted to lower temperatures for shallow cracked specimens as compared to deeply cracked specimens. This temperature shift is about 60°C for a crack length ratio of the order of 0.07.
2.) The loss of constraint effect associated with the plasticity at the top of the specimen produces a significant reduction in the maximum principal stress. The counter-balancing effect between this stress reduction and the increase in plastic zone size is well accounted for by using the probabilistic local approach.

ACKNOWLEDGEMENTS

Financial support from Electricité de France (EDF) is gratefully acknowledged.

REFERENCES

(1) J.D.G. Sumpter, Fatigue Fract. Engng. Mater. Struct., Vol. 10, 1987, pp.479-493.

(2) J.D.G. Sumpter: An experimental investigation of the T stress approach in *Constraint effects in fracture*, ASTM Symposium, Indianapolis, May 8-9, 1991.

(3) M.G. Daves, R.H. Legatt and G. Slater: An international research project to develop shallow crack fracture mechanics tests - European contribution, Welding Institute Report 5574/20/90, 1990.

(4) W.A. Sorem, R.H. Dodds and S.T. Rolfe, Int. J. Fract., Vol. 47, 1991, pp.105-126.

(5) A.M. Al-Ani and J.W. Hancock, J. Mech. Phys. Solids, Vol. 39, 1991, pp.23-43.

(6) Z.Z. Du and J.W. Hancock, J. Mech. Phys. Solids., Vol. 39, 1991, pp.555-567.

(7) N.P. O'Dowd and C.F. Shih, J. Mech. Phys. Solids., Vol. 39, 1991, pp.989-1015.

(8) N.P. O'Dowd and C.F. Shih, J. Mech. Phys. Solids., Vol. 40, 1992, pp. 939-963.

(9) Y.Y.Wang and D.M. Parks, Shallow crack fracture mechanics - Toughness tests and applications, Paper 33, Cambridge, U.K., 23-24 Sept. 1992.

(10) M.DiFant, and F.Mudry, Shallow crack fracture mechanics - Toughness tests and applications, Paper 27, Cambridge, U.K., 23-24 Sept. 1992.

(11) F.M. Beremin, Met.Trans, Vol. 14A, 1983, pp. 2277-2287.

(12) K. Wallin, T. Saario and K. Torronen, Metal Science, Vol. 18, 1984, pp.13-16.

(13) F.Mudry, F.Di Rienzo and A.Pineau, ASTM STP 995, 1989, pp. 24 - 39.

(14) J.C. Chardes and S.H. Masson, Internal report, HT/PV D 564 MAT/T 43.

(15) R.M. McMeeking, J. Mech. Phys. Solids, 1977, Vol. 25, pp. 357 to 381.

(16) C.F. Shih: Tables of Hutchinson-Rice-Rosengreen, Singular Field quantities. Materials Research Laboratory, Brown University, RI, June 1983.

(17) ASTM Standards, 1987, Standard test method for determining J-R curves, Annual Book of ASTM Standards, Section 3, Vol. 0.3 01, pp. 1129-1145.

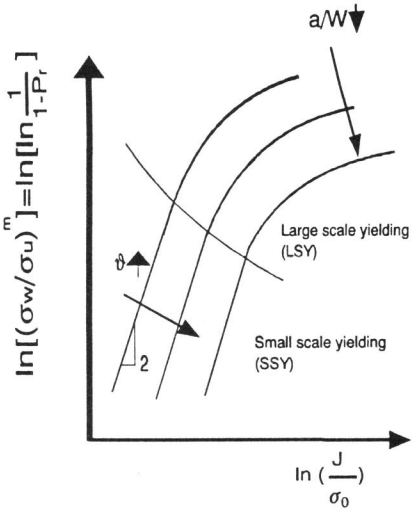

Figure 1: Loss of constraint effect (a/W↓, ϑ↑) in a Weibull diagramm

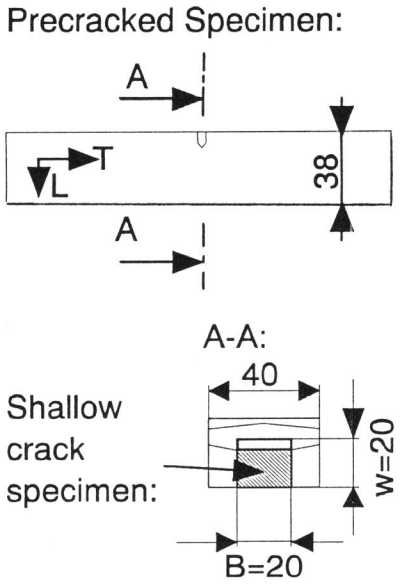

Figure 2: Fabrication of shallow cracked specimen

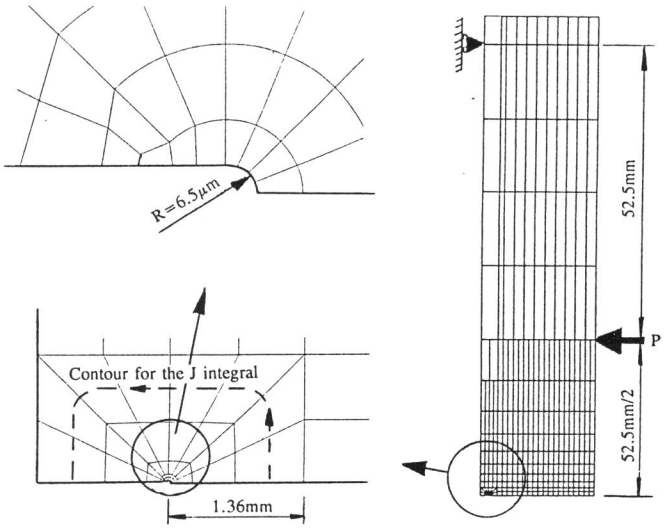

Figure 3: FE-mesh used for modelling the shallow crack specimen T84-10

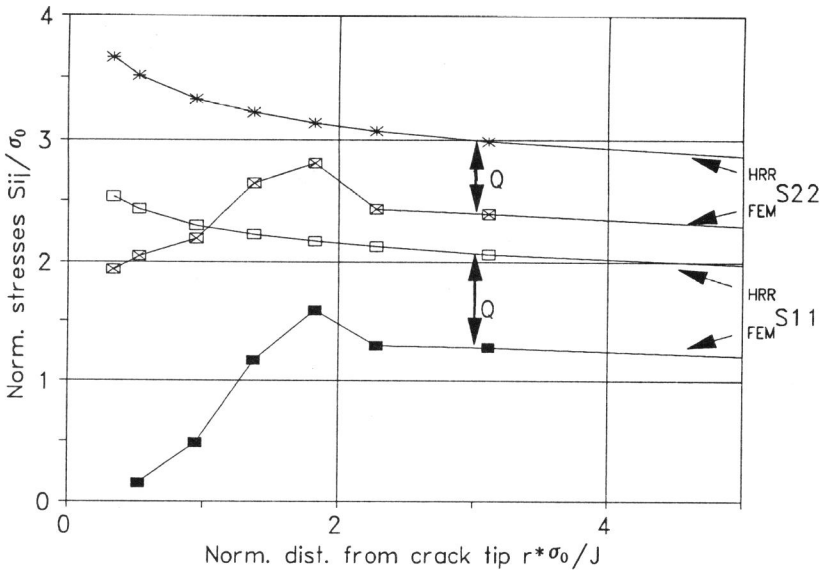

Figure 4: Stress distribution at the crack tip modelled with a finite initial radius of 6.5μm (specimen T84-10)

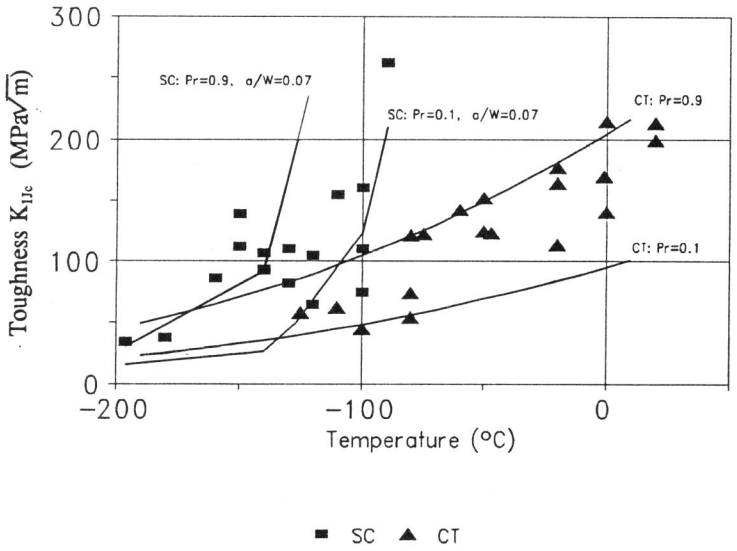

Figure 5: Transition temperature shift due to the shallow crack (SC) effect (a/W=0.07). The probabilities to failure of Pr=0.1 and Pr=0.9 are indicated.